Progress In Electromagnetics Research M, Vol. 65, 175–186, 2018

Analysis of Diffraction Graphene Gratings Using the C-Method and Design of a Terahertz Polarizer

Farzaneh A. Juneghani, Abolghasem Z. Nezhad*, and Reza Safian

Abstract—We analyze relief graphene gratings by the coordinate transformation method (the C-method). This method is also used for analysis of multilayer gratings with graphene sheets at the interfaces. By using this method, we are able to obtain the efficiency of deep graphene gratings with fast convergence rate while previous methods are limited to very shallow graphene gratings. Moreover, a terahertz polarizer is designed by relief graphene grating. Polarization extinction ratio and transmittance of single-layer and double-layer polarizer are simulated by the C-method. Double-layer polarizer gives extinction ratio from 22 dB to 10 dB over a frequency range of 1 GHz to 4 THz.

1. INTRODUCTION

In recent years, periodic structures of graphene have received considerable attention, such as the monolayer graphene having relief corrugations [1–3], graphene sheet with modulated optical conductivity [1–4], periodic array of graphene ribbons [5], and graphene on subwavelength dielectric gratings [6, 7]. Graphene sheets with relief surface have been analyzed [1–3] and fabricated [8–11] by different methods. In these structures, in addition to graphene conductivity, corrugation amplitudes can affect the efficiency of structure so that the increase of the groove depth causes the increase of graphene absorption [1].

Graphene, a single layer of carbon atoms arranged in a honeycomb lattice [12], has already shown unique mechanical, electric, thermal and magnetic properties [13]. Complex conductivity of graphene depends on frequency, electron relaxation time, temperature and chemical potential. The chemical potential of graphene can be dynamically altered by electric field, magnetic field and voltage gate [14,15]. Because of these characteristics, graphene has interesting applications in different frequencies [16–19]. For example, absorber, which is implemented based on graphene and light absorption, is tuned by changing the chemical potential or gate voltage [16], and polarizer, which is designed using array of graphene ribbons, is controlled by the chemical potential [17]. These structures are based on periodic structures of graphene, and they are in fact diffraction gratings.

Metal and dielectric diffraction gratings with relief surface are analyzed and simulated by developed analytical and numerical methods. For instance, the Rayleigh method was proposed to calculating the diffraction efficiency of relief gratings [20]. But this method was limited to the very shallow gratings. After this method, the integral method was developed for metal and dielectric relief gratings [21]. The advantage of the integral method is that it can deal with almost all kinds of gratings, but this method has mathematical complicacy and is difficult to be implemented and comprehend. Also, the coordinate transformation method (the C-method) was proposed for metal gratings with relief surface [22]. It was then extended to multilayer dielectric and metal gratings [23]. This method allows us to determine transmittance, reflectance and absorbance of the structure and it can be used for deep gratings.

Received 29 October 2017, Accepted 6 February 2018, Scheduled 15 March 2018

* Corresponding author: Abolghasem Zeidaabadi-Nezhad (zeidabad@cc.iut.ac.ir).

The authors are with the Department of Electrical and Computer Engineering, Isfahan University of Technology, Isfahan 8415683111, Iran.

Relief gratings are known to diffract and absorb electromagnetic waves. When these structures are covered with a graphene sheet, their efficiency can be dynamically tuned by electrostatic gatings. Relief graphene gatings are investigated by the Rayleigh method [2] and resonance perturbation theory [1]. But, as mentioned earlier, these methods can only be used for very shallow gratings. It must be added that commercial electromagnetic (EM) solvers often model graphene with a thin dielectric layer that its permittivity is proportional to the thickness of layer. As a result, these solvers need fine meshing that causes very slow convergence rate and memory consuming [24]. Therefore, we need a rigorous and efficient method for solving these problems.

In this paper, diffraction from the graphene sheet on the corrugated dielectric grating is analyzed using the coordinate transformation method (C-method). Here, the graphene sheet that is located at the interface between two homogeneous isotropic media is modeled with its surface conductivity. The problem is also studied for multilayer gratings with the graphene sheets at the interfaces. Obtained results of this method for graphene gratings are compared with results of the Rayleigh method and commercial EM solver. The absorbance of the light is reported for different depths of the grating. Increasing depth of the grating leads to absorbance enhancement, due to more coupling between electromagnetic radiation and surface plasmon polaritons.

Finally, a TM-pass polarizer is designed and simulated in terahertz region. The structure is formed by two sinusoidal graphene gratings with a subwavelength period. Results demonstrate that we can achieve better extinction ratio by increasing depth of the grating, the chemical potential and number of layer of the graphene gratings. Final extinction ratio for designed double-layer polarizer is from 22 dB to 10 dB over a frequency range of 1 GHz to 4 THz.

2. DESCRIPTION OF THE PROBLEM

A surface relief grating is shown in Fig. 1(a). The corrugated interface is periodic in the x direction and uniform in the z direction. The period and depth of grating are d and h, respectively, and a continuous function $a(x)$ describes the grating surface profile. A graphene sheet with the conductivity σ is placed at the interface between two homogeneous isotropic media with the refractive indexes n_1 and n_2 that n_1 is real but n_2 can be complex. The magnetic permeabilities of both media can be different but it is assumed the same with vacuum permeability. The grating is illuminated by a plane wave with an incident angle θ with respect to the Oy axis, and incident wave vector is placed in the Oxy plane.

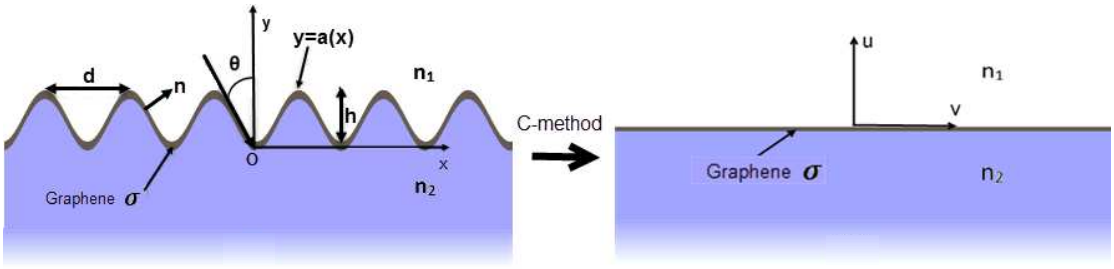

Figure 1. A surface relief grating with a graphene sheet is placed at the interface between two media (a) in the cartesian coordinates, (b) in the curvilinear coordinates.

There are two cases of TM (magnetic field vector is parallel to the Oz axis) and TE (electric field vector is parallel to the Oz axis) polarizations. Here only TM polarization is considered, although TE polarization is also similar. Since the structure is uniform in the z direction, the problem is two-dimensional, and the wave equation is as follows:

$$(\partial_x^2 + \partial_y^2 + k^2)F = 0, \tag{1}$$

where $k = \omega\sqrt{\mu_0\epsilon}$ is the wave number and $F = H_z$. As seen in Fig. 1(a), space is divided into two semi-infinite spaces by grating-profile function $a(x)$, and two domains called $D1$ and $D2$ are formed at

superstrate and substrate, respectively. By assuming a time dependence of $\exp(-i\omega t)$, the total fields in both domains can be written in Rayleigh expansions [25]

$$F(x,y) = \sum_{m=-\infty}^{m=+\infty} A_m^{(p)\pm} \exp\left(i\alpha_m x \pm i\beta_m^{(p)} y\right), \qquad p=1,\ 2, \tag{2}$$

where

$$\alpha_m = n_1 k_0 \sin\theta + mK, \qquad \beta_m^{(p)^2} = n_p^2 k_0^2 - \alpha_m^2, \tag{3}$$

in which $K = 2\pi/d$, $k_0 = 2\pi/\lambda$, λ is wavelength in vacuum; p is devoted to domains $D1$ and $D2$ with $p=1$ and $p=2$, respectively; $A_m^{(p)\pm}$ are unknown coefficients that are found. There are two cases of modes: modes propagate or decay in the positive direction of y and modes propagate or decay in the negative direction of y. These modes are shown by superscript of $+$ and $-$, respectively.

2.1. Description of the Eigenvalue Problem by the C-Method

The coefficients of $A_m^{(p)\pm}$ are obtained by satisfying the boundary conditions of problem, but this is difficult for the corrugated surface. The C-method applies boundaries of structure to curvilinear coordinate surfaces (Fig. 1(b)). Therefore, new variables are introduced by transformation

$$v = x, \qquad u = y - a(x). \tag{4}$$

Using the new variables gives the chain rule:

$$\partial_x = \partial_v - \dot{a}\partial_u, \qquad \partial_y = \partial_u, \tag{5}$$

in which $\dot{a} = da/dx$. Substituting (5) into (1) gives

$$\left((1+\dot{a}\dot{a})\,\partial_u^2 - \dot{a}\partial_v\partial_u - \partial_v\dot{a}\partial_u + \partial_v^2 + k^2\right) F = 0. \tag{6}$$

The second order propagation equation can be rewritten as a pair of first order equations

$$\begin{bmatrix} k^2+\partial_v^2 & 0 \\ 0 & 1 \end{bmatrix} \begin{bmatrix} F \\ \partial_u F \end{bmatrix} = -\partial_u \begin{bmatrix} \dot{a}\partial_v + \partial_v\dot{a} & 1+\dot{a}\dot{a} \\ -1 & 0 \end{bmatrix} \begin{bmatrix} F \\ \partial_u F \end{bmatrix}. \tag{7}$$

Because the coefficients of this equation are independent of u, we can write the u dependence as $\exp(i\rho u)$ for F and $\partial_u F$. Then $\dot{a}$ is expanded into Fourier series and we make transformations $\partial_v = i\alpha$ and $\partial_u = i\rho$; therefore, Eq. (7) is converted to a matrix equation in Fourier space as [26]

$$\begin{bmatrix} \boldsymbol{\beta}^{(p)^2} & \mathbf{0} \\ \mathbf{0} & \boldsymbol{I} \end{bmatrix} \begin{bmatrix} \boldsymbol{F} \\ \dot{\boldsymbol{F}} \end{bmatrix} = \rho \begin{bmatrix} -\dot{\boldsymbol{a}}\boldsymbol{\alpha} - \boldsymbol{\alpha}\dot{\boldsymbol{a}} & \boldsymbol{I} + \dot{\boldsymbol{a}}\dot{\boldsymbol{a}} \\ \boldsymbol{I} & \mathbf{0} \end{bmatrix} \begin{bmatrix} \boldsymbol{F} \\ \dot{\boldsymbol{F}} \end{bmatrix}, \tag{8}$$

where $\mathbf{I}$ is the identity matrix, $\mathbf{0}$ the null matrix, $\dot{\boldsymbol{a}}$ the Toeplitz matrix by Fourier coefficients of $\dot{a} = da/dx$, and $\boldsymbol{\alpha}$ and $\boldsymbol{\beta}^{(p)}$ are diagonal matrices [26]. By solving the generalized matrix eigenequation in Eq. (8) in both domains $p=1$ and $p=2$, the eigenvalues ρ and eigenvectors $\begin{bmatrix} \boldsymbol{F} \\ \dot{\boldsymbol{F}} \end{bmatrix}$ can be obtained. For the numerical solution of eigenvalue problem in Eq. (8), we truncate the infinite matrices and introduce an integer M and let m runs from $-M$ to M, so that the size of submatrices in Eq. (8) will be $(2M+1)\times(2M+1)$. The $4M+2$ eigenvalues can be determined and divided into sets that will be discussed in next section. Thus the total magnetic fields in both domains $p=1$ and $p=2$ are written as

$$\begin{aligned} F^{(p)} &= F^{(p)^+} + F^{(p)^-} \\ &= \sum_{m=-M}^{m=+M} \exp(i\alpha_m v) \sum_{q=-M}^{q=+M} F_{mq}^{(p)^+} \exp\left(i\rho_q^{(p)} u\right) B_q^{(p)^+} \\ &\quad + \sum_{m=-M}^{m=+M} \exp(i\alpha_m v) \sum_{q=-M}^{q=+M} F_{mq}^{(p)^-} \exp\left(i\rho_q^{(p)} u\right) B_q^{(p)^-}, \qquad p=1,\ 2, \end{aligned} \tag{9}$$

where $F_{mq}^{(p)\pm}$ are elements of qth eigenvector of the generalized matrix eigenequation in Eq. (8).

2.2. Boundary Conditions

The unknown coefficients $B_q^{(p)^{\pm}}$ can be determined by matching the tangential components of fields on the surface $u = 0$. Since in this problem a graphene sheet is placed at the interface between two media, the boundary conditions will be different from Fig. 1 without graphene sheet. The graphene sheet is modeled with its surface conductivity, and proper boundary conditions are applied [27],

$$\boldsymbol{n} \times (\boldsymbol{E}_1 - \boldsymbol{E}_2) = 0, \qquad \boldsymbol{n} \times (\boldsymbol{H}_1 - \boldsymbol{H}_2) = \sigma \boldsymbol{E}_t, \tag{10}$$

in which the subscript t is for defining the tangential component of electric field, and $\boldsymbol{n}$ is the unit normal vector to the interface in Fig. 1. The tangential component of electric field is given by $E_t = \boldsymbol{E}.\boldsymbol{t}$. The unit tangent vector $\boldsymbol{t}$ is obtained from the gradient on the grating surface with profile function $a(x)$. Therefore, we have

$$G = E_t = \frac{1}{\sqrt{1+\dot{a}^2}} E_x + \frac{\dot{a}}{\sqrt{1+\dot{a}^2}} E_y, \tag{11}$$

where the tangential component of electric field is denoted by G, for convenient mathematical manipulations in the next sections. From Maxwell's equations $E_x = -(Z_0/ik_0\epsilon)\partial_y H_z$ and $E_y = (Z_0/ik_0\epsilon)\partial_x H_z$, where $Z_0 = (\mu_0/\epsilon_0)^{(1/2)}$, and Eq. (5) we can express G as

$$G = \frac{Z_0}{ik_0\epsilon} \left[\frac{\dot{a}}{\sqrt{1+\dot{a}^2}} \partial_v F - \sqrt{1+\dot{a}^2}\, \partial_u F \right]. \tag{12}$$

By substituting Eq. (9) in Eq. (12) we have

$$G_{mq}^{(p)^{\pm}} = \frac{Z_0}{k_0 \epsilon_{(p)}} \sum_s \left[(\dot{a})_{m-s} ((\sqrt{I + \dot{\boldsymbol{a}}.\dot{\boldsymbol{a}}})^{-1})_{ms} \alpha_s - (\sqrt{I + \dot{\boldsymbol{a}}.\dot{\boldsymbol{a}}})_{ms} \rho_q^{(p)} \right] F_{sq}^{(p)^{\pm}}, \tag{13}$$

where $\dot{\boldsymbol{a}} \cdot \dot{\boldsymbol{a}}$ denotes the matrix multiplication, and $\sqrt{\boldsymbol{I} + \dot{\boldsymbol{a}} \cdot \dot{\boldsymbol{a}}}$ denotes a matrix $\boldsymbol{Y}$ such that $\boldsymbol{Y} \cdot \boldsymbol{Y} = \boldsymbol{I} + \dot{\boldsymbol{a}} \cdot \dot{\boldsymbol{a}}$, and $\dot{\boldsymbol{a}}$ is a matrix with the elements that are Fourier coefficients of $\dot{a}$ such that

$$(\dot{\boldsymbol{a}})_{ms} = (\dot{a})_{m-s} = \frac{1}{d} \int_0^d \dot{a}(x) \exp[-i(m-s)Kx]\, dx. \tag{14}$$

By using boundary conditions in Eq. (10) and scattering matrix (S-matrix) which connects input waves to output waves [28] and is defined as

$$\begin{bmatrix} \boldsymbol{B}_q^{(1)^+} \\ \\ \boldsymbol{B}_q^{(2)^-} \end{bmatrix} = \boldsymbol{S} \begin{bmatrix} \boldsymbol{B}_q^{(2)^+} \\ \\ \boldsymbol{B}_q^{(1)^-} \end{bmatrix}, \tag{15}$$

we have

$$\boldsymbol{S} = \begin{bmatrix} \boldsymbol{F}^{(1)^+} - \sigma \boldsymbol{G}^{(1)^+} & -\boldsymbol{F}^{(2)^-} \\ \\ \boldsymbol{G}^{(1)^+} & -\boldsymbol{G}^{(2)^-} \end{bmatrix}^{-1} \begin{bmatrix} \boldsymbol{F}^{(2)^+} & \sigma \boldsymbol{G}^{(1)^-} - \boldsymbol{F}^{(1)^-} \\ \\ \boldsymbol{G}^{(2)^+} & -\boldsymbol{G}^{(1)^-} \end{bmatrix} = \begin{bmatrix} \boldsymbol{S}_{11} & \boldsymbol{S}_{12} \\ \\ \boldsymbol{S}_{21} & \boldsymbol{S}_{22} \end{bmatrix}, \tag{16}$$

where $\boldsymbol{F}^{(p)^{\pm}}$ and $\boldsymbol{G}^{(p)^{\pm}}$ are submatrices with elements $F_{mq}^{(p)^{\pm}}$ and $G_{mq}^{(p)^{\pm}}$, respectively. In this problem, $\boldsymbol{B}_q^{(p)^{\pm}}$ are column matrices which consist of $2M+1$ elements that determine constant amplitudes. Because of Sommerfeld conditions for diffracted fields, we have $B_q^{(2)^+} = 0$ for all q and $B_q^{(1)^-} = 0$ for all q, except $q = 0$, and we assume $B_0^{(1)^-} = 1$. The eigenvalues have two sets: real and complex. Real eigenvalues and corresponding eigenvectors are denoted with U which give near field and far field; complex eigenvalues and corresponding eigenvectors are denoted with V which give only near field. With this notation, the eigenvectors are rewritten as

$$\boldsymbol{F}^{(p)^{\pm}} = \boldsymbol{F}_U^{(p)^{\pm}} + \boldsymbol{F}_V^{(p)^{\pm}}, \qquad \boldsymbol{G}^{(p)^{\pm}} = \boldsymbol{G}_U^{(p)^{\pm}} + \boldsymbol{G}_V^{(p)^{\pm}}. \tag{17}$$

As expressed in detail by Chandezon [26], elements of eigenvectors with subscript U are as follows:

$$F_{mq,U}^{(p)\ \pm} = L_{m-q}\left(\pm\beta_q^{(p)}\right), \qquad q \in U, \tag{18}$$

$$G_{mq,U}^{(p)} = \frac{Z_0}{k_0\epsilon_{(p)}}\sum_s \left[(\dot{\boldsymbol{a}})_{m-s}((\sqrt{I+\dot{\boldsymbol{a}}.\dot{\boldsymbol{a}}})^{-1})_{ms}\alpha_s \mp (\sqrt{I+\dot{\boldsymbol{a}}.\dot{\boldsymbol{a}}})_{ms}\beta_q^{(p)}\right] \times L_{m-q}\left(\pm\beta_q^{(p)}\right), \qquad q \in U, \tag{19}$$

where $\beta_r^{(p)}$ are real Rayleigh eigenvalues and are equal to real eigenvalues $\rho_q^{(p)}$ [26]. L_{m-q} is defined as

$$L_{m-q}\left(\pm\beta_q^{(p)}\right) = \frac{1}{d}\int_0^d \exp\left[\pm i\beta_q^{(p)}a\left(x\right) - i(m-q)Kx\right]dx. \tag{20}$$

The incident wave is the corresponding eigenvector of the eigenvalue of $B_1^{(1)^-}$ and is assumed as $\begin{bmatrix} \boldsymbol{I}' \\ \boldsymbol{I}'' \end{bmatrix}$, where

$$I'_m = L_m\left(-\beta_0^{(1)}\right), \tag{21}$$

$$I''_m = \frac{Z_0}{k_0\epsilon_{(1)}}\sum_s \left[(\dot{a})_{m-s}((\sqrt{I+\dot{\boldsymbol{a}}.\dot{\boldsymbol{a}}})^{-1})_{ms}\alpha_s + (\sqrt{I+\dot{\boldsymbol{a}}.\dot{\boldsymbol{a}}})_{ms}\beta_0^{(1)}\right] L_m\left(-\beta_0^{(1)}\right). \tag{22}$$

Therefore, field in domain $p=1$ is expressed as

$$\begin{bmatrix} \boldsymbol{F}^{(1)^+} & \boldsymbol{F}^{(1)^-} \\ \boldsymbol{G}^{(1)^+} & \boldsymbol{G}^{(1)^-} \end{bmatrix}\begin{bmatrix} \boldsymbol{B}_q^{(1)^+} \\ \boldsymbol{B}_q^{(1)^-} \end{bmatrix} = \begin{bmatrix} \boldsymbol{F}_U^{(1)^+} & \boldsymbol{F}_V^{(1)^+} & \boldsymbol{0} \\ \boldsymbol{G}_U^{(1)^+} & \boldsymbol{G}_V^{(1)^+} & \boldsymbol{0} \end{bmatrix}\begin{bmatrix} \boldsymbol{B}_{q,U}^{(1)^+} \\ \boldsymbol{B}_{q,V}^{(1)^+} \\ \boldsymbol{0} \end{bmatrix} + \begin{bmatrix} \boldsymbol{I}' \\ \boldsymbol{I}'' \end{bmatrix}, \tag{23}$$

where $\boldsymbol{B}_{q,U}^{(1)^+}$ and $\boldsymbol{B}_{q,V}^{(1)^+}$ are unknown coefficients corresponding to real and complex eigenvalues (with size of P and $2M+1-P$), respectively. for simplicity we have

$$\begin{bmatrix} \boldsymbol{F}^{(1)^+} & \boldsymbol{F}^{(1)^-} \\ \boldsymbol{G}^{(1)^+} & \boldsymbol{G}^{(1)^-} \end{bmatrix} = \begin{bmatrix} \boldsymbol{F}_{11} & \boldsymbol{F}_{12} \\ \boldsymbol{G}_{11} & \boldsymbol{G}_{12} \end{bmatrix}, \qquad \begin{bmatrix} \boldsymbol{F}'_{11} \\ \boldsymbol{G}'_{11} \end{bmatrix} = \begin{bmatrix} \boldsymbol{F}_U^{(1)^+} & \boldsymbol{F}_V^{(1)^+} \\ \boldsymbol{G}_U^{(1)^+} & \boldsymbol{G}_V^{(1)^+} \end{bmatrix}, \qquad \boldsymbol{R} = \begin{bmatrix} \boldsymbol{B}_{q,U}^{(1)^+} \\ \boldsymbol{B}_{q,V}^{(1)^+} \end{bmatrix}, \tag{24}$$

where $\boldsymbol{F}'_{11}$ and $\boldsymbol{G}'_{11}$ have size of $(2M+1)\times(2M+1)$. From Eqs. (15) and (16) we have

$$\boldsymbol{B}_q^{(1)^+} = \boldsymbol{S}_{12}\boldsymbol{B}_q^{(1)^-}, \qquad \boldsymbol{B}_q^{(2)^-} = \boldsymbol{S}_{22}\boldsymbol{B}_q^{(1)^-}. \tag{25}$$

Therefore, $\boldsymbol{R}$ and $\boldsymbol{B}_q^{(2)^-}$ are yielded with substituting Eqs. (24) and (25) in Eq. (23)

$$\boldsymbol{R} = \left[\boldsymbol{F}'_{11} - (\boldsymbol{F}_{11}\boldsymbol{S}_{12}+\boldsymbol{F}_{12})(\boldsymbol{G}_{11}\boldsymbol{S}_{12}+\boldsymbol{G}_{12})^{-1}\boldsymbol{G}'_{11}\right]^{-1}\left[(\boldsymbol{F}_{11}\boldsymbol{S}_{12}+\boldsymbol{F}_{12})\left(\boldsymbol{F}_{11}\boldsymbol{S}_{12}+\boldsymbol{G}_{12}\right)^{-1}\boldsymbol{I}'' - \boldsymbol{I}'\right], \tag{26}$$

$$\boldsymbol{B}_q^{(2)^-} = \boldsymbol{S}_{22}(\boldsymbol{G}_{11}\boldsymbol{S}_{12}+\boldsymbol{G}_{12})^{-1}(\boldsymbol{G}'_{11}\boldsymbol{R}+\boldsymbol{I}''). \tag{27}$$

Also, in the other domain ($p=2$), there are two sets of modes, propagating and decaying. Therefore, the coefficients $\boldsymbol{B}_q^{(2)^-}$ can be divided into $\boldsymbol{B}_{q,U}^{(2)^-}$ and $\boldsymbol{B}_{q,V}^{(2)^-}$. The eigenvectors in domain $p=2$ are rewritten as

$$\begin{bmatrix} \boldsymbol{F}^{(2)^+} & \boldsymbol{F}^{(2)^-} \\ \boldsymbol{G}^{(2)^+} & \boldsymbol{G}^{(2)^-} \end{bmatrix}\begin{bmatrix} \boldsymbol{B}_q^{(2)^+} \\ \boldsymbol{B}_q^{(2)^-} \end{bmatrix} = \begin{bmatrix} \boldsymbol{0} & \boldsymbol{F}_U^{(2)^-} & \boldsymbol{F}_V^{(2)^-} \\ \boldsymbol{0} & \boldsymbol{G}_U^{(2)^-} & \boldsymbol{G}_V^{(2)^-} \end{bmatrix}\begin{bmatrix} \boldsymbol{0} \\ \boldsymbol{B}_{q,U}^{(2)^-} \\ \boldsymbol{B}_{q,V}^{(2)^-} \end{bmatrix}, \tag{28}$$

where $\boldsymbol{B}_{q,U}^{(2)^-}$ and $\boldsymbol{B}_{q,V}^{(2)^-}$ are unknown coefficients corresponding to real and complex eigenvalues (with size of Q and $2M+1-Q$), respectively. For simplicity we have

$$\begin{bmatrix} \boldsymbol{F}^{(2)^+} & \boldsymbol{F}^{(2)^-} \\ \boldsymbol{G}^{(2)^+} & \boldsymbol{G}^{(2)^-} \end{bmatrix} = \begin{bmatrix} \boldsymbol{F}_{21} & \boldsymbol{F}_{22} \\ \boldsymbol{G}_{21} & \boldsymbol{G}_{22} \end{bmatrix}, \qquad \begin{bmatrix} \boldsymbol{F}'_{22} \\ \boldsymbol{G}'_{22} \end{bmatrix} = \begin{bmatrix} \boldsymbol{F}_U^{(2)^-} & \boldsymbol{F}_V^{(2)^-} \\ \boldsymbol{G}_U^{(2)^-} & \boldsymbol{G}_V^{(2)^-} \end{bmatrix}, \qquad \boldsymbol{T} = \begin{bmatrix} \boldsymbol{B}_{q,U}^{(2)^-} \\ \boldsymbol{B}_{q,V}^{(2)^-} \end{bmatrix}, \tag{29}$$

where $\boldsymbol{F}'_{22}$ and $\boldsymbol{G}'_{22}$ have size of $(2M+1)\times(2M+1)$. The coefficients $\boldsymbol{T}$ can be determined using [28] as

$$\boldsymbol{Z} = \begin{bmatrix} \boldsymbol{F}_{21} & \boldsymbol{F}_{22} \\ \boldsymbol{G}_{21} & \boldsymbol{G}_{22} \end{bmatrix}^{-1} \begin{bmatrix} \boldsymbol{F}_{21} & \boldsymbol{F}'_{22} \\ \boldsymbol{G}_{21} & \boldsymbol{G}'_{22} \end{bmatrix} = \begin{bmatrix} \boldsymbol{I} & \boldsymbol{0} \\ \boldsymbol{0} & \boldsymbol{Z}_{22} \end{bmatrix}, \tag{30}$$

$$\boldsymbol{T} = {\boldsymbol{Z}_{22}}^{-1} \boldsymbol{B}_q^{(2)^-}. \tag{31}$$

Finally, the diffraction efficiencies η_q^r and η_q^t are obtained as the following:

$$\eta_q^r = \frac{\beta_q^{(1)}}{\beta_0^{(1)}} \left| B_{q,U}^{(1)^+} \right|^2, \qquad \eta_q^t = \frac{\epsilon_2 \beta_q^{(2)}}{\epsilon_1 \beta_0^{(1)}} \left| B_{q,U}^{(2)^-} \right|^2. \tag{32}$$

2.3. Multilayer Gratings

A multilayer grating is shown in Fig. 2. There are Q layers with the refractive indexes n_j, and thickness of each layer is e_j $(j=0,\ldots,Q)$. Profile function of surfaces is as

$$y_j = -\sum_{i=1}^{j} e_i + a(x). \tag{33}$$

For generality, we have supposed that graphene sheets with the conductivities of σ_j are placed on all the surfaces of y_j. We present S-matrix for the structure as the follows:

$$\begin{bmatrix} \boldsymbol{B}_q^{(0)^+} \\ \boldsymbol{B}_q^{(Q+1)^-} \end{bmatrix} = \boldsymbol{S}(Q+1,0) \begin{bmatrix} \boldsymbol{B}_q^{(Q+1)^+} \\ \boldsymbol{B}_q^{(0)^-} \end{bmatrix}. \tag{34}$$

T-matrix which couples the coefficient matrices of $\boldsymbol{B}_q^{(j)^+}$, $\boldsymbol{B}_q^{(j)^-}$ and $\boldsymbol{B}_q^{(j+1)^+}$, $\boldsymbol{B}_q^{(j+1)^-}$ helps to determine S-matrix in Eq. (34) as

$$\begin{bmatrix} \boldsymbol{B}_q^{(j+1)^+} \\ \boldsymbol{B}_q^{(j+1)^-} \end{bmatrix} = \boldsymbol{T}(j) \begin{bmatrix} \boldsymbol{B}_q^{(j)^+} \\ \boldsymbol{B}_q^{(j)^-} \end{bmatrix}. \tag{35}$$

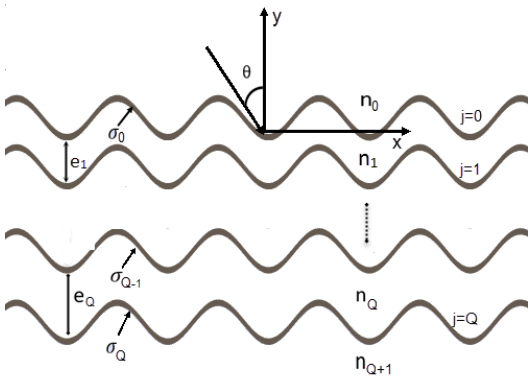

Figure 2. A multilayer grating with graphene sheets with the conductivities of σ_j that are placed on the surfaces of y_j.

Using the boundary conditions in previous section for graphene sheet, matrix $\boldsymbol{T}$ is obtained as the follows:

$$\boldsymbol{T}(j) = \boldsymbol{I}(j)^{-1}\boldsymbol{M}(j), \tag{36}$$

where

$$\boldsymbol{I}(j) = \begin{bmatrix} \exp\left(i\rho_1^{(j)}e_j\right) & \ddots & \boldsymbol{0} \\ \boldsymbol{0} & & \exp\left(i\rho_{4M+2}^{(j)}e_j\right) \end{bmatrix}, \tag{37}$$

$$\boldsymbol{M}(j) = \begin{bmatrix} \boldsymbol{F}^{(j+1)^+} & \boldsymbol{F}^{(j+1)^-} \\ \boldsymbol{G}^{(j+1)^+} & \boldsymbol{G}^{(j+1)^-} \end{bmatrix}^{-1} \begin{bmatrix} \boldsymbol{F}^{(j)^+} - \sigma_j \boldsymbol{G}^{(j)^+} & \boldsymbol{F}^{(j)^-} - \sigma_j \boldsymbol{G}^{(j)^-} \\ \boldsymbol{G}^{(j)^+} & \boldsymbol{G}^{(j)^-} \end{bmatrix}, \tag{38}$$

where $\boldsymbol{I}(j)$ is a diagonal matrix. S-matrix can be obtained for multilayer grating using T-matrix:

$$\begin{aligned} \boldsymbol{S}_{11}(0, j+1) &= [\boldsymbol{T}_{11}(j) - \boldsymbol{S}_{12}(0,j)\boldsymbol{T}_{21}(j)]^{-1}\boldsymbol{S}_{11}(0,j), \\ \boldsymbol{S}_{12}(0, j+1) &= [\boldsymbol{T}_{11}(j) - \boldsymbol{S}_{12}(0,j)\boldsymbol{T}_{21}(j)]^{-1}[\boldsymbol{S}_{12}(0,j)\boldsymbol{T}_{22}(j) - \boldsymbol{T}_{12}(j)], \\ \boldsymbol{S}_{21}(0, j+1) &= [\boldsymbol{S}_{22}(0,j)\boldsymbol{T}_{21}(j)\boldsymbol{S}_{11}(0,j+1) + \boldsymbol{S}_{21}(0,j)], \\ \boldsymbol{S}_{22}(0, j+1) &= [\boldsymbol{S}_{22}(0,j)\boldsymbol{T}_{21}(j)\boldsymbol{S}_{12}(0,j+1) + \boldsymbol{S}_{22}(0,j)\boldsymbol{T}_{22}(j)], \end{aligned} \tag{39}$$

where $\boldsymbol{S}_{11}, \ldots, \boldsymbol{S}_{22}$ and $\boldsymbol{T}_{11}, \ldots, \boldsymbol{T}_{22}$ are submatrices of $\boldsymbol{S}$ and $\boldsymbol{T}$ matrices, and the size of any submatrix is $(2M+1) \times (2M+1)$. It is obvious that $\boldsymbol{S}(0,0)$ is a identity matrix. Therefore, we can start from $\boldsymbol{S}(0,0)$ and obtain $\boldsymbol{S}(0, Q+1)$ by Eq. (39). After determination of $\boldsymbol{S}(0, Q+1)$, we can continue from Eqs. (17) to (32) and change subscripts of (1) and (2) to (0) and $(Q+1)$, respectively. Eventually, the diffraction coefficients of Eq. (32) are obtained.

3. NUMERICAL RESULTS

In this section, to verify the validity of analysis of graphene grating using C-method, the example in [2] is revisited, and its results are compared with results of C-method and a commercial EM solver. The surface conductivity of graphene is obtained using [29]:

$$\sigma = i\frac{e^2 k_B T}{\pi\hbar^2(\omega + i\tau^{-1})}\left[\frac{\mu_c}{k_B T} + 2\ln\left(\exp\left(-\frac{\mu_c}{k_B T}\right) + 1\right)\right] + i\frac{e^2}{4\pi}\ln\left[\frac{2|\mu_c| - (\omega + i\tau^{-1})}{2|\mu_c| + (\omega + i\tau^{-1})}\right], \tag{40}$$

where μ_c is the chemical potential, T the temperature, e the electron charge, $\hbar$ the reduced Planck's constant, and τ the momentum relaxation time [29]. The structure is shown in Fig. 1. The grating profile is $a(x) = (h/2)\sin(2\pi x/d)$ with period $d = 10\,\mu\text{m}$. The graphene sheet is placed at the interface between two media with refractive indexes of $n_1 = 1$ and $n_2 = 3.3$. The chemical potential of $\mu_c = 0.45\,\text{eV}$ and the electron scattering rate of $\Gamma = 2.6\,\text{meV}$ or, equivalently, $\tau = 1/(2\Gamma) = 0.25\,\text{ps}$ are assumed for graphene. The grating is illuminated by the TM wave at the normal incident angle. This structure has been analyzed by the Rayleigh method in [2]. Note that in this case since period of gratings is smaller than wavelength of incident wave, $d \ll \lambda$, we have only zero order diffraction. Transmittance, reflectance and absorbance for different depths of grating are shown in Fig. 3 using the C-method, EM solver and Rayleigh method [2]. For implementation of the C-method the truncation order of $M = 5$ is selected. As seen in Fig. 3, results of the three methods are the same when depth of grating is low ($h = d/12.5$). However, with increasing the depth of grating ($h = d/5$), the difference between the C-method and Rayleigh method increases, but there is good agreement between the C-method and EM solver. Because the Rayleigh method is appropriate for shallow gratings, when depth of grating becomes larger than $h = d/5$, results of the Rayleigh method start to fail [2]. However, the C-method is not limited by deep gratings. It gives accurate results for deep gratings until $h/d \simeq 3$ [23].

For comparison of the convergence rate and accuracy of the C-method and Rayleigh method for graphene gratings, the relative error of the absorbance of previous sinusoidal graphene grating with two different depths at 3 THz frequency is computed as a function of the truncation order. Fig. 4 illustrates

the percent relative error of both methods. The reference values of error are calculated by assuming the converged results ($M = 40$). Firstly, the relative error of graphene grating with the depth of $h = 0.2d$ is determined. As shown in Fig. 4, C-method has an excellent percent relative error for truncation orders of larger than $M = 3$. For the Rayleigh method, an excellent percent relative error is obtained for truncation orders of larger than $M = 3$. The relative error decreases by increasing the truncation order of two methods, but the C-method has faster convergence rate. For depth of $h = 0.6d$, the result of the Rayleigh method cannot converge with increasing the truncation order while C-method is able to simulate the deeper grating with good convergence rate and a relative error below 1%, with truncation orders of larger than $M = 5$. The total CPU time to calculate the efficiency of graphene grating at 45 data points in Fig. 2, with truncation orders of $M = 5$, is 7.48 sec.

Effect of the depth of graphene grating (Fig. 1) is investigated. In Fig. 5, the absorbances of structure by the C-method and EM solver are shown for different depths of the grating. Period of grating is $d = 20\,\mu$m, and the refractive indexes are $n_1 = 1$ and $n_2 = 1.97$. The parameters of graphene

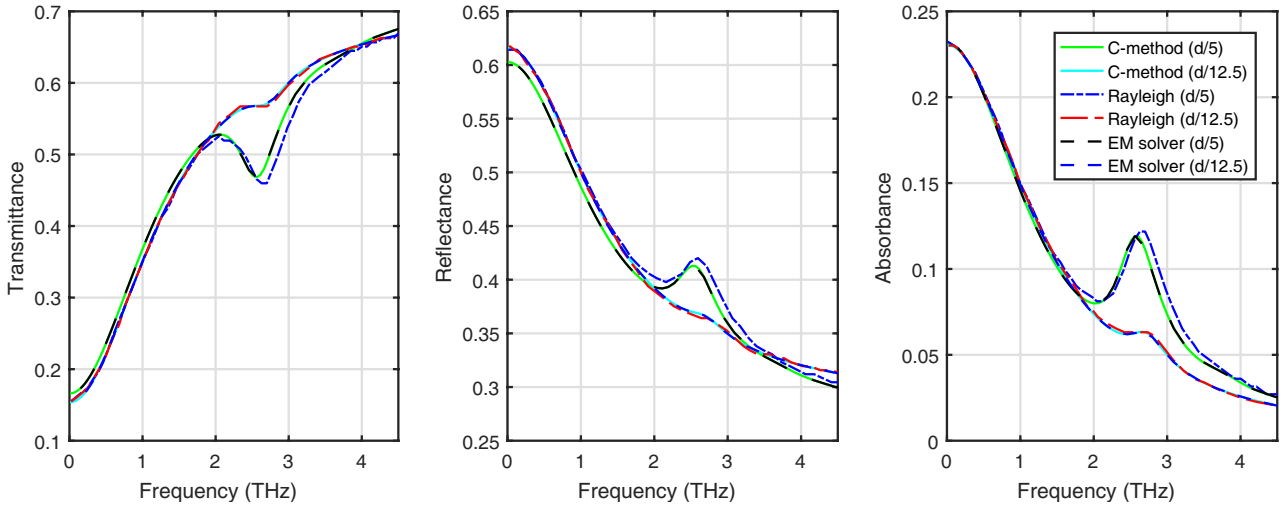

Figure 3. Comparison of transmittance, reflectance and absorbance for different depths of a graphene grating by the C-method, the Rayleigh method and EM solver.

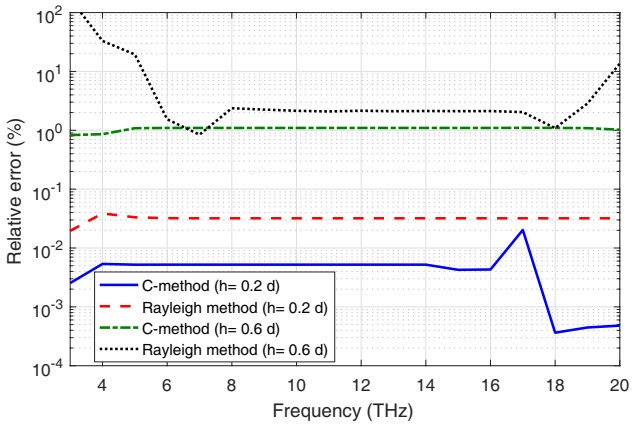

Figure 4. Relative errors in computation of absorption curve vs. truncation order for different depths of a grating graphene.

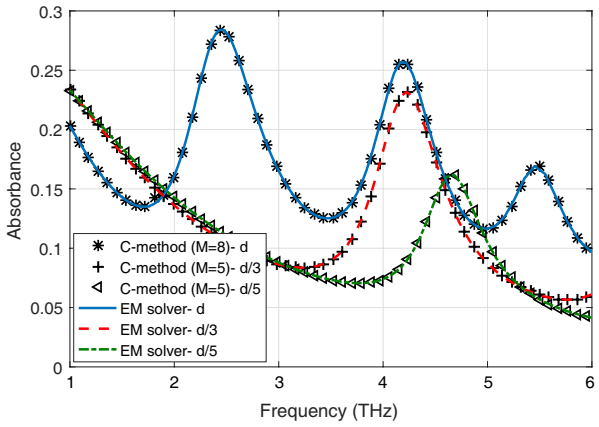

Figure 5. Absorbance for different depths of a sine grating with deep grooves that a graphene sheet is placed onto the two media with refractive indexes of $n_1 = 1$ and $n_2 = 3.3$.

are assumed $\mu_c = 0.6\,\text{eV}$ and $\Gamma = 2.6\,\text{meV}$. As shown in Fig. 5, the absorbance peak is increased with deeper gratings, because the coupling between electromagnetic radiation and graphene plasmons is enhanced as the depth of grooves is increased. Also, agreement between results of the C-methods and EM solver is good.

4. DESIGN OF A TERAHERTZ POLARIZER

In this section, a terahertz polarizer using graphene is designed by the C-method. Its schematic has been proposed in Fig. 6. The structure is formed by two layers of the relief graphene gratings with the profile function of $a(x) = (h/2)\sin(2\pi x/d)$. They are placed on silica (SiO_2). The period of the structure is $d = 2\,\mu\text{m}$, and depth is $h = 2\,\mu\text{m}$. Space between graphene sheets is $e_1 = 10\,\mu\text{m}$, and the refractive index of SiO_2 is 1.97. The thickness of $500\,\mu\text{m}$ is chosen for substrate. The parameters of graphene are assumed as $\mu_c = 1\,\text{eV}$ and $\Gamma = 0.11\,\text{meV}$ [30, 31]. The polarizer is illuminated by the incident plane waves with TM and TE polarizations. The incident angle of the plane wave is θ.

The transmittance of the structure is simulated for single-layer and double-layer structures. The

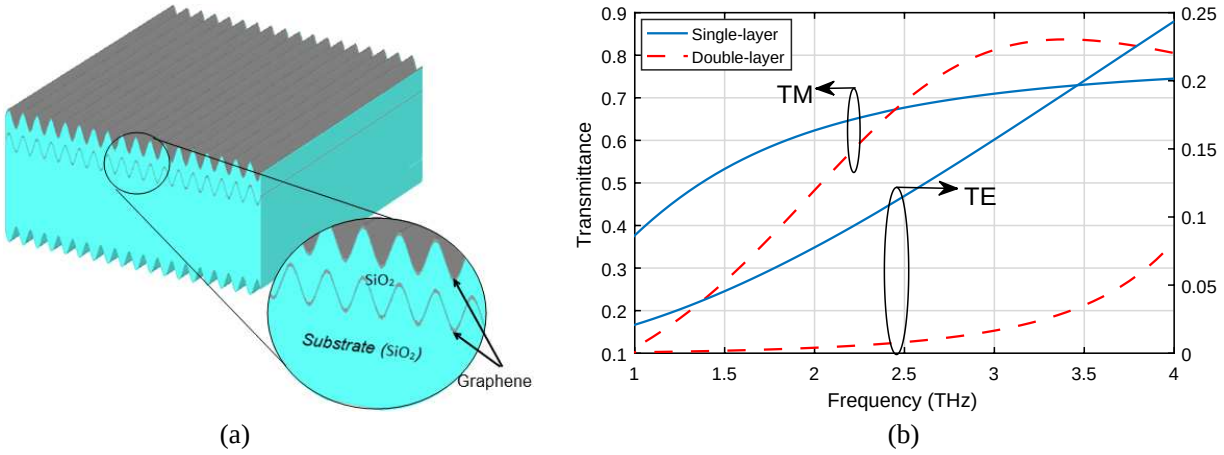

Figure 6. (a) Polarizer structure is formed by two layers of graphene gratings, with sine profile function, on the SiO_2 substrate. (b) TM and TE transmittance of the polarizer with different layer of graphene vs. frequency.

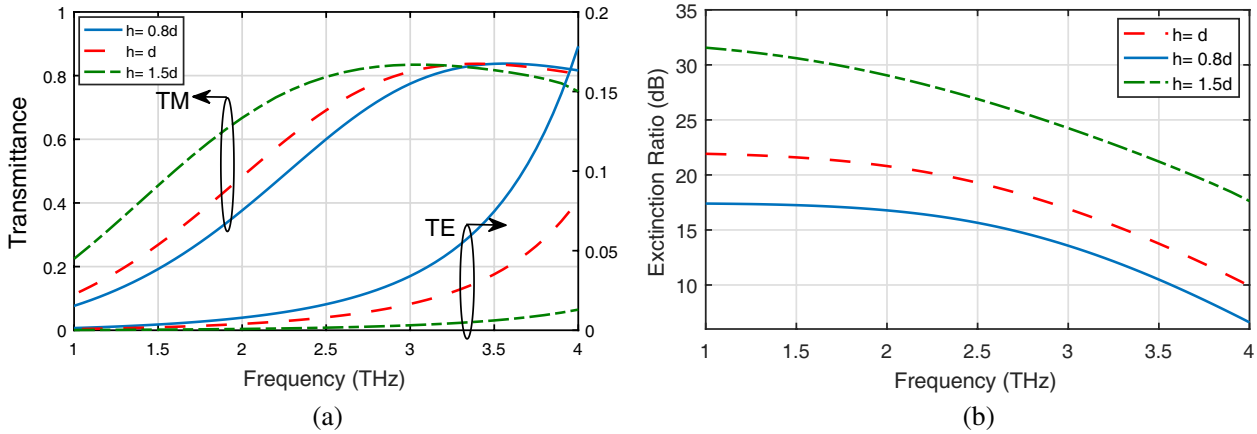

Figure 7. (a) TM and TE transmittance (b) and extinction ratio of the polarizer for different depth of grooves vs. frequency.

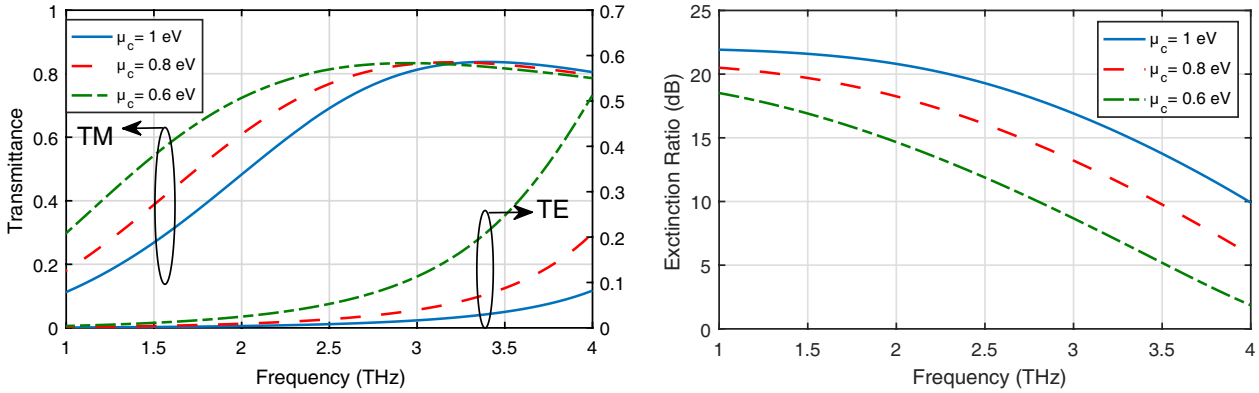

Figure 8. (a) TM and TE transmittance (b) and extinction ratio of the polarizer for different chemical potential vs. frequency.

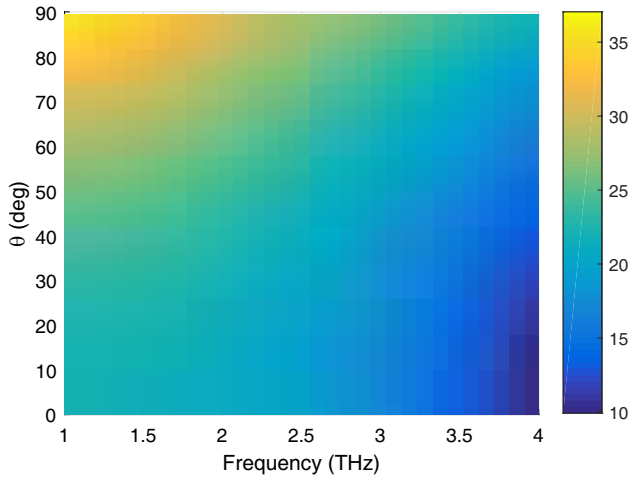

Figure 9. Extinction ratio of the polarizer vs. frequency at different incident angles.

results of TM and TE polarizations are shown in Fig. 6(b). The transmittance of TE polarization decreases by increasing number of graphene gratings. For TM polarization, we have increasing transmittance for high frequencies by double-layer structure. In addition to the number of grating layers, depth of grating also affects the transmittance of two polarizations (Fig. 7). As seen in Fig. 7(a), the transmittance of TE wave decreases with deeper gratings, but the transmittance of TM wave increases. The TM transmittance of the double-layer polarizer for the depth of $h = d$ is more than 60% over a frequency range of 2.5–4 THz. Extinction ratio for different depth at normal incident is shown in Fig. 7(b) which is defined as $10\log_{10}(T_{TM}/T_{TE})$. Deeper grating ($h = 1.5d$) gives better extinction ratio at the frequency range of 1–4 THz. The depth of $h = d$ is selected, because of manufacturing considerations [8, 11]. The extinction ratio is more than 10 dB for $h = d$.

Also, the efficiency of the designed polarizer can be tuned by varying the chemical potential of graphene via the external voltage. The results of TM and TE transmittances for different chemical potentials are shown in Fig. 8(a). The TE transmittance decreases by increasing the chemical potential, and the average TM transmittance increases. The extinction ratio is reported in Fig. 8(b) which demonstrates that the performance of the polarizer improves.

This polarizer gives a better performance at higher incident angle. The extinction ratio is presented from $\theta = 0$ to $\theta = 90°$ in Fig. 9. It is shown that the extinction ratio is improved with increasing the incident angle at the frequency range from 1–4 THz for incident angle up to $\theta = 90°$.

5. CONCLUSION

In this paper, we use coordinate transformation method to analyze the diffraction graphene gratings. The graphene sheet is modeled with its surface conductivity, and the suitable boundary conditions are applied. For numerical stability, S-matrix is used. Also, the problem is extended to multilayer gratings with the graphene sheets at the interface between two media. This method is able to analyze the deep graphene diffraction gratings accurately, and results are in good agreement with EM solver, but the Rayleigh method is divergent for deep gratings and is limited to very shallow gratings. Results of C-method are in good agreement with EM solver. The absorbance of graphene grating is increased with deep grooves for the single-layer graphene grating, with sine profile function. In addition, the transmittance and extinction ratio for TM and TE polarizations are investigated by different parameters for a terahertz polarizer. It is observed that the extinction ratio is enhanced by increasing number of the graphene layer, depth of the grooves and the chemical potential.

REFERENCES

1. Slipchenko, T. M., M. L. Nesterov, L. Martin-Moreno, and A. Yu Nikitin, "Analytical solution for the diffraction of an electromagnetic wave by a graphene grating," *J. Opt.*, Vol. 15, 114008, 2013.
2. Bludov, Y. V., A. Ferreira, N. M. R. Peres, and M. I. Vasilevskiy, "A primer on surface plasmon-polaritons in graphene," *Int. J. of Mod. Phys. B*, Vol. 27 1341001, 2013.
3. Peres, N. M. R., A. Ferreira, Y. V. Bludov, and M. I. Vasilevskiy, "Light scattering by a medium with a spatially modulated optical conductivity: the case of graphene," *J. Phys.: Condens. Matter*, Vol. 24, 245303, 2012.
4. Huidobro, P. A., M. Kraft, R. Kun, S. A. Maier, and J. B. Pendry, "Graphene, plasmons and transformation optics," *J. Opt.*, Vol. 18, 044024, 2016.
5. Nikitin, A. Y., F. Guinea, F. J. Garcia-Vidal, and L. Martin-Morene, "Surface plasmon enhanced absorption and suppressed transmission in periodic arrays of graphene ribbons," *Phys. Rev.*, Vol. 85, 081405, 2011.
6. Zhan, T. R., F. Y. Zhao, X. H. Hu, X. H. Liu, and J. Zi, "Band structure of plasmons and optical absorption enhancement in graphene on subwavelength dielectric gratings at infrared frequencies," *Phys. Rev. B*, Vol. 86, 165416, 2012.
7. Peres, N. M. R., Y. V. Bludov, A, Ferreira, and M. I. Vasilevskiy, "Exact solution for square-wave grating covered with graphene: surface plasmon-polaritons in the terahertz range," *J. Phys.:Condens. Matter*, Vol. 25 125303, 2013.
8. Ding, J., F. T. Fisher, and E. H. Yang, "Direct transfer of corrugated graphene sheets as stretchable electrodes," *Journal of Vacuum Science and Technology B, Nanotechnology and Microelectronics: Materials, Processing, Measurement, and Phenomena*, Vol. 34, 051205, 2016.
9. Wang, M., J. Leem, P. Kang, J. Choi, P. Knapp, K. Yong, and S. Nam, "Mechanical instability driven self-assembly and architecturing of 2D materials," *2D Materials*, Vol. 4, 022002, 2017.
10. Yan, Z. X., Y. L. Zhang, W. Wang, X. Y. Fu, H. B. Jiang, Y. Q. Liu, P. Verma, S. Kawata, and H. B. Sun, "Superhydrophobic SERS substrates based on silver-coated reduced graphene oxide gratings prepared by two-beam laser interference," *ACS Applied Materials and Interfaces*, Vol. 7, 27059, 2015.
11. Florio, G. D., E. Brundermann, N. S. Yadavalli, S. Santer, and M. Havenith "Graphene multilayer as nano-sized optical strain gauge for polymer surface relief gratings," *Nano Letters*, Vol. 14, 5754, 2014.
12. Novoselov, K. S., A. K. Geim, S. V. Morozov, D. Jiang, Y. Zhang, S. V. Dubonos, I. V. Grigorieva, and A. A. Firsov, "Electric field effect in atomically thin carbon films," *Science*, Vol. 306, 666, 2004.
13. Jablan, M., M. Soljacic, and H. Buljan, "Plasmons in graphene: fundamental properties and potential applications," *Proc. IEEE*, Vol. 101, 1689, 2013.

14. Gusynin, P., S. G. Sharapov, and J. P. Carbotte, "Magneto-optical conductivity in graphene," *J. Phys.: Condens. Matter*, Vol. 19, 026222, 2007.
15. Li, Z. Q., E. A. Henriksen, Z. Jiang, Z. Hao, M. C. Martin, P. Kim, H. L. Stormer, and D. N. Basov, "Dirac charge dynamics in graphene by infrared spectroscopy," *Nature Phys.*, Vol. 4, 532, 2008.
16. Alaee, R., M. Farhat, C. Rockstuhl, and F. Lederer, "A perfect absorber made of a graphene micro-ribbon metamaterial," *Opt. Express*, Vol. 20, 28017, 2012.
17. Fadakar, H., A. Borji, A. Z. Nezhad, and M, Shahabadi, "Improved fourier analysis of periodically patterned graphene sheets embedded in multilayered structures and its application to the design of a broadband tunable wide-angle polarizer," *IEEE J. Quantum Electron*, Vol. 53, 1, 2017.
18. Khoozani, P. K., M. Maddahali, M. Shahabadi, and A. Bakhtafrouz, "Analysis of magnetically biased graphene-based periodic structures using a transmission-line formulation," *JOSA B*, Vol. 33, 2566, 2016.
19. Kim, J. T. and S. Y. Choi, "Graphene-based plasmonic waveguides for photonic integrated circuits," *Opt. Express*, Vol. 19, 24557, 2011.
20. Rayleigh, L., "On the dynamical theory of grating," *Proc. R. Soc. A*, Vol. 79, 399, 1907.
21. Maystre, D. and M. Neviere, "Electromagnetic theory of crossed gratings," *J. Opt.*, Vol. 9, 301, 1978.
22. Chandezon, J., D. Maystre, and G. Raoult, "A new theoretical method for diffraction gratings and its numerical application," *J. Opt.*, Vol. 11, 235, 1980.
23. Chandezon, J., M. T. Dupuis, G. Cornet, and D. Maystre, "Multicoated gratings: a differential formalism applicable in the entire optical region," *J. Opt. Soc. Am.*, Vol. 72, 839, 1982.
24. Cao, Y. S., L. J. Jiang, and L. J. Ruehli, "The derived equivalent circuit model for non-magnetized and magnetized graphene," *In Wireless Information Technology and Systems (ICWITS) and Applied Computational Electromagnetics (ACES), 2016 IEEE/ACES International Conference on*, 1, 2016.
25. Petit, R. *A Tutorial Introduction*, Electromagnetic Theory of Gratings. Springer Berlin Heidelberg, 1980.
26. Li, L, J. Chandezon, G. Granet, and J.-P. Plumey, "Rigorous and efficient grating-analysis method made easy for optical engineers," *Appl. Opt.*, Vol. 38, 304, 1999.
27. David, J. G. and R. College, *Introduction to Electrodynamics*, Prentice Hall, 1999.
28. Ko, D. Y. K. and J. R. Sambles, "Scattering matrix method for propagation of radiation in stratified media: attenuated total reflection studies of liquid crystals," *J. Opt. Soc. Am. A*, Vol. 5, 1863, 1988.
29. Chen, P. Y. and A. Alu, "Atomically thin surface cloak using graphene monolayers," *ACS Nano*, Vol. 5, 5855, 2011.
30. Hanson, G. W., "Dyadic Green's functions and guided surface waves for a surface conductivity model of graphene," *J. Appl. Phys.*, Vol. 103, 064302, 2008.
31. Jishi, R. A., M. S. Dresselhaus, and G. Dresselhaus, "Electron-phonon coupling and the electrical conductivity of fullerene nanotubules," *Phys. Rev. B*, Vol. 48, 11385, 1993.